

## Element abundance ratios in the quiet Sun transition region

P.R. YOUNG<sup>1,2,3</sup>

<sup>1</sup>*College of Science, George Mason University, 4400 University Drive, Fairfax, VA 22030, USA*

<sup>2</sup>*Code 671, NASA Goddard Space Flight Center, Greenbelt, MD 20771, USA*

<sup>3</sup>*Northumbria University, Newcastle Upon Tyne, NE1 8ST, UK*

### ABSTRACT

Element abundance ratios of magnesium to neon (Mg/Ne) and neon to oxygen (Ne/O) in the transition region of the quiet Sun have been derived by re-assessing previously published data from the Coronal Diagnostic Spectrometer on board the Solar and Heliospheric Observatory in the light of new atomic data. The quiet Sun Mg/Ne ratio is important for assessing the effect of magnetic activity on the mechanism of the first ionization potential (FIP) effect, while the Ne/O ratio can be used to infer the solar photospheric abundance of neon, which can not be measured directly. The average Mg/Ne ratio is found to be  $0.52 \pm 0.11$ , which applies over the temperature region 0.2–0.7 MK, and is consistent with the earlier study. The Ne/O ratio is, however, about 40% larger, taking the value  $0.24 \pm 0.05$  that applies to the temperature range 0.08–0.40 MK. The increase is mostly due to changes in ionization and recombination rates that affect the equilibrium ionization balance. If the Ne/O ratio is interpreted as reflecting the photospheric ratio, then the photospheric neon abundance is  $8.08 \pm 0.09$  or  $8.15 \pm 0.10$  (on a logarithmic scale for which hydrogen is 12), according to whether the oxygen abundances of M. Asplund et al. or E. Caffau et al. are used. The updated photospheric neon abundance implies a Mg/Ne FIP bias for the quiet Sun of  $1.6 \pm 0.6$ .

*Keywords:* Sun: abundances — Sun: transition region — Sun: UV radiation — Sun:photosphere

### 1. INTRODUCTION

Young (2005a,b) used EUV spectra from the Coronal Diagnostic Spectrometer (CDS) on board the Solar and Heliospheric Observatory (SOHO) to derive element abundance ratios of magnesium to neon (Mg/Ne) and neon to oxygen (Ne/O) in the quiet Sun, and an update to the Mg/Ne results was presented by Young (2006). The derived values applied to the upper transition region ( $\approx 0.1$ –0.7 MK) and were unique in that they were the first to be obtained in this temperature region on the solar disk rather than at the solar limb. Quiet Sun measurements of the Mg/Ne ratio at the limb were made with the Mg VI and Ne VI ions by Feldman & Widing (1993), Dwivedi et al. (1999) and Doschek & Laming (2000), but the latter paper noted that the temperature structure shows large changes over small distances just above the limb, which can modify the derived Mg/Ne abundance ratio. The temperature structure on the solar disk does not show such large variations with spatial position, while the availability of multiple ions for each element from the CDS spectra removes the dependence on individual ions.

The Mg/Ne ratio is important for investigating the so-called FIP effect in the solar atmosphere, the finding that elements with first ionization potentials (FIPs)  $\leq 10$  eV are over-abundant compared to elements with FIPs larger than this value (e.g., Feldman & Laming 2000). The nature of the transition at this boundary is uncertain, and Schmelz et al. (2012) adopted a linear transition between 9 and 11 eV. Magnesium is a low-FIP element (7.6 eV), and neon and oxygen are high-FIP elements (21.6 and 13.6 eV, respectively). The Ne/O ratio is of interest because it potentially allows the photospheric abundance of neon to be determined if it is assumed that the atmospheric ratio represents the photospheric value (since neon and oxygen are both considered high-FIP). This is significant because the photospheric neon abundance can not be directly determined since the element has no useful absorption lines in the photospheric spectrum. The Mg/Ne FIP bias—the amount by which the ratio is enhanced or depleted compared to the photospheric value—depends on the photospheric neon abundance, hence the need to measure Ne/O.

The present work revisits the analyses of Young (2005a,b) using updated atomic data available in the CHIANTI atomic database (Young et al. 2016), with a

particular focus on changes in the equilibrium ionization fractions that have arisen since 2005. Firstly, ionization and recombination rate coefficients have been updated, and secondly a formula for computing the suppression of dielectronic recombination as density increases has been published (Nikolić et al. 2013).

The observational data used here are presented in Sect. 2. Sect. 3 discusses the current status of photospheric abundances for oxygen, neon and magnesium, and Sect. 4 highlights the connection between abundances, the standard model of the solar interior and helioseismology measurements. Sect. 5 compares the ionization equilibrium curves used in the present work with those used by Young (2005a,b), and Sect. 6 gives details of other atomic data. The method for calculating the Mg/Ne and Ne/O ratios is presented in Sect. 7, and the results are given in Sect. 8. A comparison with coronal neon and oxygen studies is given in Sect. 9, and the final results are summarized in Sect. 10.

## 2. OBSERVATIONS AND CALIBRATION

CDS consisted of a single telescope that fed two distinct spectrometers: the Grazing Incidence Spectrometer (GIS) and the Normal Incidence Spectrometer (NIS). The emission lines considered in the present work are all from the NIS: the magnesium lines all lie in the NIS1 waveband (308–379 Å) and the neon and oxygen lines all lie in the NIS2 waveband (513–633 Å). A complete list of the atomic transitions is given in Table 1. Due to self-blending at the CDS spectral resolution, individual emission features correspond to multiple atomic transitions for some ions. In these cases the emissivities for the individual transitions are summed in the atomic models.

The emission line intensity measurements of Young (2005a,b) are used, and no new measurements were performed. The quiet Sun was divided into equal spatial areas of network and supergranule cell centers based on the intensity of O v  $\lambda$ 629.7 (formed at 0.2 MK) and intensities were measured for 24 datasets between 1996 March and 1998 June. This period was prior to the temporary loss of SOHO in 1998<sup>1</sup>, after which the NIS line profiles were significantly distorted, making measurements of weak lines difficult. For the present work we derive abundance ratios for the average quiet Sun in addition to network and cell centers, and these were derived simply by averaging the network and cell center intensities, since the two regions have equal spatial areas. We refer the reader to Young (2005a,b) for further details on how the data were processed and how the lines were measured.

<sup>1</sup> <http://www.esa.int/esapub/bulletin/bullet97/vandenbu.pdf>

**Table 1.** Atomic transitions used for the analysis.

Ion	Transition	$\lambda/\text{Å}$
O III	$2s^2 2p^2 \ ^1S_0 - 2s 2p^3 \ ^1P_1$	599.59
O IV	$2s^2 2p \ ^2P_{1/2} - 2s 2p^2 \ ^2P_{3/2}$	553.33
	$2s^2 2p \ ^2P_{1/2} - 2s 2p^2 \ ^2P_{1/2}$	554.08
	$2s^2 2p \ ^2P_{3/2} - 2s 2p^2 \ ^2P_{3/2}$	554.51
O V	$2s^2 2p \ ^2P_{3/2} - 2s 2p^2 \ ^2P_{1/2}$	555.26
	$2s^2 \ ^1S_0 - 2s 2p \ ^1P_1$	629.73
Ne IV	$2s^2 2p^3 \ ^4S_{3/2} - 2s 2p^4 \ ^4P_{5/2}$	543.89
Ne v	$2s^2 2p^2 \ ^3P_2 - 2s 2p^3 \ ^3D_1$	572.03
Ne VI	$2s^2 2p \ ^2P_{3/2} - 2s 2p^2 \ ^2D_{3/2}$	562.71
	$2s^2 2p \ ^2P_{3/2} - 2s 2p^2 \ ^2D_{5/2}$	562.81
Ne VII	$2s 2p \ ^3P_1 - 2p^2 \ ^3P_1$	561.38
	$2s 2p \ ^3P_2 - 2p^2 \ ^3P_2$	561.73
Mg v	$2s^2 2p^4 \ ^3P_2 - 2s 2p^5 \ ^3P_2$	353.09
	$2s^2 2p^4 \ ^3P_1 - 2s 2p^5 \ ^3P_1$	353.30
Mg VI	$2s^2 2p^3 \ ^2D_{5/2} - 2s 2p^4 \ ^2D_{3/2}$	349.11
	$2s^2 2p^3 \ ^2D_{3/2} - 2s 2p^4 \ ^2D_{3/2}$	349.13
	$2s^2 2p^3 \ ^2D_{5/2} - 2s 2p^4 \ ^2D_{5/2}$	349.16
	$2s^2 2p^3 \ ^2D_{3/2} - 2s 2p^4 \ ^2D_{5/2}$	349.18
Mg VII	$2s^2 2p^2 \ ^3P_2 - 2s 2p^3 \ ^3P_2$	367.68
	$2s^2 2p^2 \ ^3P_2 - 2s 2p^3 \ ^3P_1$	367.69
Mg VIII	$2s^2 2p \ ^2P_{3/2} - 2s 2p^2 \ ^2P_{3/2}$	315.02

The standard radiometric calibration of NIS has not changed since 2002, and so the intensities measured by Young (2005a,b) are still valid. An alternative calibration was presented by Del Zanna et al. (2010) and we find differences of 15% or less with the standard calibration for the time period considered here, which is within the uncertainty of the NIS calibration.

## 3. PHOTOSPHERIC ABUNDANCES

In this section the current status of the photospheric abundances of oxygen, neon and magnesium is discussed. The notation used for abundances is as follows: the abundance,  $\epsilon$ , of an element X is defined as  $N(X)/N(H)$  where  $N$  is the number density. The abundance on a logarithmic scale is  $A(X) = 12 + \log \epsilon(X)$ , and it is this value that is typically given in compilations.

Asplund et al. (2009) presented abundances mostly derived from results of their 3D magnetoconvection simulations of photospheric absorption lines. Their recommended value for oxygen was  $A(O) = 8.69 \pm 0.05$ . Updates for elements heavier than oxygen were published by Scott et al. (2015b), Scott et al. (2015a) and Grevesse et al. (2015), and the magnesium abundance was  $7.59 \pm 0.04$ . The neon abundance remained un-

changed compared to [Asplund et al. \(2009\)](#), and the value of  $7.93 \pm 0.10$  was derived from the oxygen abundance by applying the Ne/O ratio of [Young \(2005b\)](#). With these values the photospheric Mg/Ne ratio is 0.47. We refer to the updated [Asplund et al. \(2009\)](#) compilation as "Asp-Sco" in the following text.

A distinct abundance compilation was created by [Lodders et al. \(2009\)](#) who were more cautious in the use of abundances derived from 3D models. The oxygen abundance was taken as  $8.73 \pm 0.07$ , a little higher than [Asplund et al. \(2009\)](#) but consistent within the error bars. For magnesium, [Lodders et al. \(2009\)](#) used the value of  $7.54 \pm 0.06$  from [Holweger \(1979\)](#)—see also [Holweger \(2001\)](#)—which is close to the meteoritic value of 7.53. The most significant difference compared to [Asplund et al. \(2009\)](#) is the neon abundance, with a value of  $8.05 \pm 0.10$ . This is an average of the value of [Morel & Butler \(2008\)](#), derived from a sample of B stars, and the solar flare value of [Landi et al. \(2007\)](#). Both of these are absolute abundance measurements, i.e., relative to hydrogen.

[Caffau et al. \(2011\)](#) calculated photospheric abundances for 12 elements using the CO5BOLD code, and suggested that these replace the values in the [Lodders et al. \(2009\)](#) compilation. Mg and Ne were not updated, but oxygen was increased to  $8.76 \pm 0.07$ . We refer to the hybrid Lodders–Caffau compilation as "Lod-Caf" in the following text.

We summarize the different abundance values and their corresponding ratios in Table 2, where we also compare with the compilation of [Grevesse & Sauval \(1998\)](#) that was made prior to the use of 3D models for photospheric line studies.

#### 4. THE STANDARD SOLAR MODEL AND HELIOSEISMOLOGY RESULTS

Prior to the updates to the photospheric abundances of the key elements carbon, nitrogen and oxygen in the early 2000's, the predictions of the standard solar model (SSM) of the solar interior were in excellent agreement with measurements of solar parameters from helioseismology. The updated abundances led to discrepancies that have not yet been resolved, and some authors argue that the discrepancies demonstrate that the updated abundances are incorrect. For example, [Villante et al. \(2014\)](#) treat the ratio of volatiles to refractory elements as a free parameter in reconciling the SSM with the helioseismology and solar neutrino results and find the ratio is more consistent with the [Grevesse & Sauval \(1998\)](#) compilation than the [Asplund et al. \(2009\)](#) compilation. Until this situation is resolved there will remain a cloud of uncertainty over the photospheric abundances of key

elements such as oxygen and neon, and these cause problems when trying to measure the FIP bias in solar atmosphere plasma.

The fact that the photospheric neon abundance is only measured indirectly led [Antia & Basu \(2005\)](#) and [Bahcall et al. \(2005\)](#) to suggest that the modeling–observation discrepancy could be resolved if the neon abundance was actually two to three times higher than previously thought. A study of stellar coronal abundances measured from *Chandra* spectra ([Drake & Testa 2005](#)) suggested this was plausible, but the subsequent study of [Robrade et al. \(2008\)](#) found that the Ne/O ratio was correlated with stellar activity, with low activity stars being consistent with the accepted solar Ne/O ratio. There remains the key question of whether the coronal Ne/O abundance actually represents the photospheric value, and we will return to this issue in Sect. 9.

#### 5. IONIZATION FRACTIONS

A standard assumption in astrophysics is that the ionization fractions of an element at any given temperature are independent of the electron density and they are often referred to as "zero-density ion fractions" as they are correct in the limiting case of density tending to zero. Prior to CHIANTI 6, scientists typically took the zero-density ion fractions from standard tabulations such as [Arnaud & Rothenflug \(1985\)](#), [Mazzotta et al. \(1998\)](#) and [Bryans et al. \(2009\)](#). With CHIANTI 6 ([Dere et al. 2009](#)), critically-assessed ionization and recombination rates were added to the database and used to compute a new ionization equilibrium dataset that is now the default option for CHIANTI. The analysis of [Young \(2005a,b\)](#) took place prior to this change, and the [Mazzotta et al. \(1998\)](#) dataset was used.

Density effects can modify the equilibrium ion fractions through the suppression of dielectronic recombination (DR) rates, which is caused by electron collisions de-populating highly-excited states prior to recombination. [Nikolić et al. \(2013\)](#) provided formulae for computing the suppression factors for astrophysically important ions, and these formulae have been implemented by the author to compute density and pressure sensitive ion fraction tables derived by applying the suppression factors to the DR rates in CHIANTI 8 ([Del Zanna et al. 2015](#)). One feature of the [Nikolić et al. \(2013\)](#) suppression factor formulae is an unphysical discontinuity of a factor two for the isoelectronic sequences hydrogen through boron (see Sect. 2.2.1 of [Nikolić et al. 2013](#)), and for O IV and O V the discontinuities occur close to the temperatures of maximum ionization of the ions. D. Nikolić (private communication, 2017) provided the

**Table 2.** Abundances and abundance ratios from select compilations.

Compilation	$A(\text{O})$	$A(\text{Ne})$	$A(\text{Mg})$	$R_{\text{Mg/Ne}}$	$R_{\text{Ne/O}}$
Grevesse & Sauval (1998)	$8.83 \pm 0.06$	$8.08 \pm 0.06$	$7.58 \pm 0.05$	$0.316 \pm 0.061$	$0.178 \pm 0.037$
Asplund et al. (2009)	$8.69 \pm 0.05$	$7.93 \pm 0.10$	$7.60 \pm 0.04$	$0.468 \pm 0.129$	$0.174 \pm 0.050$
Asp-Sco	$8.69 \pm 0.05$	$7.93 \pm 0.10$	$7.59 \pm 0.04$	$0.457 \pm 0.126$	$0.174 \pm 0.050$
Lodders et al. (2009)	$8.73 \pm 0.07$	$8.05 \pm 0.10$	$7.54 \pm 0.06$	$0.309 \pm 0.092$	$0.209 \pm 0.065$
Lod-Caf	$8.76 \pm 0.07$	$8.05 \pm 0.10$	$7.54 \pm 0.06$	$0.309 \pm 0.092$	$0.195 \pm 0.061$

author with an updated formula that smooths out this discontinuity and also provides an improved fit to the original data for these sequences. This formula was applied in the present work.

Figure 1 compares the ion fractions computed at a pressure of  $10^{14.5} \text{ K cm}^{-3}$  with those from Mazzotta et al. (1998), and significant differences are found for several of the ions. For example, O III and O IV are shifted to lower temperatures by 0.1 dex, and the ion fraction of Mg VI is 30% lower. The differences are a combination of the updated ionization and recombination data distributed with CHIANTI and the changes introduced by DR suppression. Appendix A discusses the differences between the new pressure equilibrium dataset and the CHIANTI 8 file.

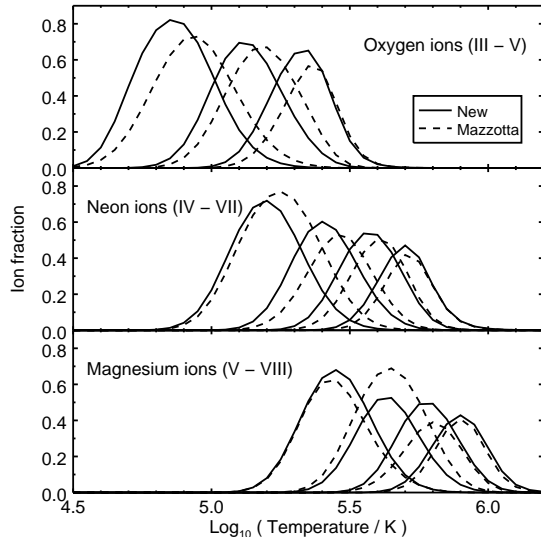


**Figure 1.** Ion fraction plots for the oxygen, neon and magnesium ions studied in the present work. The solid lines show the curves derived for a pressure of  $10^{14.5} \text{ K cm}^{-3}$ ; the dashed lines show the curves from Mazzotta et al. (1998).

## 6. OTHER ATOMIC DATA

The atomic data for computing emissivities are all taken from CHIANTI 8 (Del Zanna et al. 2015), with

the exception of Ne VI. An error in the data files was found for this ion, whereby levels 6 and 7 ( $2s2p^2 \ ^2D_{3/2,5/2}$ ) were mis-labeled, and these levels give rise to the  $\lambda 562.71$  and  $\lambda 562.81$  transitions that are measured in the CDS spectra. The modified Ne VI files will be released with the next version of the database.

The initial study of the Mg/Ne ratio (Young 2005a) made use of CHIANTI 4, and the results were updated by Young (2006) using CHIANTI 5. This version was also used by Young (2005b) for the Ne/O ratio. Since CHIANTI 5, all of the ions considered in the present work have been updated, except for Ne VII, Mg V and Mg VI. Further details are given in the papers that describe versions 6, 7, 7.1 and 8 of the database (Dere et al. 2009; Landi et al. 2012, 2013; Del Zanna et al. 2015, respectively).

## 7. METHOD

The model for the emission line intensities is a slightly modified version of the one used by Young (2005a,b), which writes the intensity,  $I$ , as a sum of isothermal plasma components:

$$I = \epsilon \sum_k G(T_k, N_{e,k}) N_{e,k} N_{H,k} h_k \quad (1)$$

where  $G$  is the contribution function,  $N_H$  and  $N_e$  are the number densities of hydrogen and electrons, respectively,  $T$  is the plasma temperature, and  $h$  is the plasma column depth. The sum is performed over temperatures uniformly spaced on a  $\log T$  grid. The contribution function contains the atomic physics parameters, which are all taken from CHIANTI 8, and it is derived using the GOFNT procedure in the CHIANTI IDL software with the /NOABUND keyword set and with the ion fraction file described in Sect. 5.

A constant pressure,  $P = N_e T = 10^{14.5} \text{ K cm}^{-3}$ , is assumed, based on the coronal density measured in the quiet Sun by Young (2005a). This was derived using a Si IX density diagnostic and only small changes to the CHIANTI atomic model have been since CHIANTI 4 (see Dere et al. 2009; Landi et al. 2012) and these had a negligible impact on the diagnostic. For the present

work the temperature grid has a spacing of 0.05 dex. The previous work used 0.1 dex intervals, and the change reflects the improvement in resolution of the ionization equilibrium files distributed with the more recent versions of CHIANTI.

In order that a  $\chi^2$  minimization technique can be applied, we define the column depth distribution simply by making the  $h$  values at the start, middle and end of the temperature range to be free parameters. We refer to these three values as  $p_1$ ,  $p_2$  and  $p_3$  and the temperatures at which they are defined are  $\log T = 5.0, 5.6$  and  $6.1$  for the Mg/Ne method, and  $4.5, 5.2$  and  $5.8$  for the Ne/O method. All other  $h$  values on the temperature grid are obtained by drawing straight lines between  $p_1$  and  $p_2$ , and  $p_2$  and  $p_3$  in  $\log T$ – $\log h$  space. Figure 2 shows examples of the derived  $h$  distributions. For the Mg/Ne calculation, the four fitting parameters are adjusted to achieve the best agreement with the eight observed Mg and Ne emission lines, while for the Ne/O calculation there are six emission lines (Ne VII is not included as it has negligible overlap with the three oxygen ions—see Figure 1). There is one emission line from each ion, and the atomic transitions are given in Table 1, where we note that some lines consist of multiple transitions at the CDS spectral resolution. The minimization procedure was performed with the MPFIT IDL routines (Markwardt 2009), which yielded  $1\sigma$  error bars on the abundance ratios and  $p_i$  values.

If we consider the example of determining the Ne/O relative abundance ratio, then we write the intensities of the neon and oxygen lines at wavelengths  $\lambda$  by

$$I_{\lambda, \text{Ne}} = R_{\text{Ne/O}} \epsilon(\text{O}) f_{\lambda}(p_1, p_2, p_3) \quad (2)$$

$$I_{\lambda, \text{O}} = \epsilon(\text{O}) f_{\lambda}(p_1, p_2, p_3) \quad (3)$$

where we use  $f_{\lambda}$  to indicate the sum in Eq. 1, and  $R_{\text{Ne/O}} = \epsilon(\text{Ne})/\epsilon(\text{O})$ . The free parameters are then  $R_{\text{Ne/O}}$ ,  $p_1$ ,  $p_2$  and  $p_3$ , and a least squares fit is performed to minimize the difference between the observed intensities and the  $I_{\lambda}$  values. Examples of the  $p_1$ ,  $p_2$  and  $p_3$  values derived for the Mg/Ne and Ne/O methods for one CDS dataset are shown in Figure 2.

We highlight that the abundance of oxygen enters into Eqs. 2 and 3 as a fixed parameter. We take this, and the abundance of neon for the Mg/Ne case, from the Lod-Caf abundance compilation. This choice does not affect the final abundance ratio, as can be seen by considering Eq. 3. Scaling  $\epsilon(\text{O})$  by some factor  $\alpha$  requires that  $f(\lambda)$  be scaled downwards by  $\alpha$ , and thus  $R_{\text{Ne/O}}$  in Eq. 2 is unaffected. The derived column depths are affected, however. For example, if the Asp-Sco neon abundance was used instead for the Mg/Ne method, then the col-

umn depths would be 32% larger to compensate for the lower neon abundance (Table 2).

One change compared to the earlier analyses is the use of the correct temperature-dependent value for the ratio  $N_{\text{H}}/N_{\text{e}}$  that is derived using the element abundance and ionization equilibrium files using the CHIANTI routine PROTON\_DENS. The ratio shows a negligible variation between the various photospheric abundance datasets, and we choose the Lod-Caf set here. Finally, a mistake in the previous method was corrected whereby line emissivities were computed at constant density rather than constant pressure, although this has a minor effect on the results.

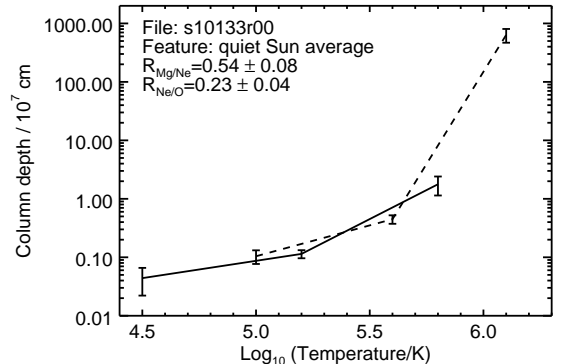


**Figure 2.** Column depth distributions for one CDS dataset are shown, as derived with the Ne/O (solid line) and Mg/Ne (dashed line) methods. The points with the error bars correspond to the  $p_1$ ,  $p_2$  and  $p_3$  values that are derived from the minimization method—see main text.

## 8. RESULTS

For each of the 24 CDS datasets we apply the minimization method to determine the Ne/O and Mg/Ne relative abundance ratios for the average quiet Sun, and the network and cell center regions separately, using the sets of oxygen, neon and magnesium lines. Young (2005a,b) demonstrated that the ratios show no systematic variation with time and this does not change here, so we only discuss the ratio values averaged over the 24 datasets.

### 8.1. The Ne/O ratio

The average Ne/O abundance ratios for network and cell center are  $0.239 \pm 0.010$  and  $0.258 \pm 0.012$ , respectively. The difference between these values only has a  $1.2\sigma$  significance and so for the remainder of this section we consider only the average quiet Sun value, which is  $0.244 \pm 0.010$ . This is about 40% higher than that derived by Young (2005b), and the difference mostly lies with the change in the ion fractions. If we use the origi-



nal [Mazzotta et al. \(1998\)](#) ion fraction file, but interpolated onto a 0.05 dex grid in temperature (to be compatible with the modern files), then we find a ratio of 0.183, which is only 10% higher than the [Young \(2005b\)](#) value. With the zero-density ion fraction file distributed with CHIANTI 8, the value is 0.237 and so the largest part of the increase comes from the changes to ionization and recombination rates between [Mazzotta et al. \(1998\)](#) and the CHIANTI 8 ion balance calculation.

The small uncertainty on the Ne/O ratio comes from the standard deviation of the values derived from the 24 datasets. The uncertainties in the atomic data are likely the biggest source of errors, as reflected in the large change to the Ne/O ratio found here, but they are difficult to quantify. Here we assign a 20% uncertainty that, when combined with the statistical error, gives a final quiet Sun Ne/O ratio of  $0.244 \pm 0.050$ .

If we now interpret this average quiet Sun value as representing the photospheric ratio, then we have the choice of the [Asplund et al. \(2009\)](#) oxygen value, or the [Caffau et al. \(2011\)](#) value. The former results in a neon abundance of  $A(\text{Ne}) = 8.08 \pm 0.09$ , while the latter yields  $A(\text{Ne}) = 8.15 \pm 0.10$ .

Noting that [Asplund et al. \(2009\)](#) used our previous result to derive the neon abundance, we suggest this compilation be updated with the value  $A(\text{Ne}) = 8.08 \pm 0.09$ . As mentioned in Sect. 3, the compilation of [Lodders et al. \(2009\)](#) took the neon abundance from two absolute measurements, rather than ratio values.

### 8.2. The Mg/Ne ratio

The average Mg/Ne ratios for quiet Sun network and cell center regions are  $0.497 \pm 0.035$  and  $0.609 \pm 0.077$ , which are 15–25% larger than those of [Young \(2005a\)](#), but only marginally different to the updated values of [Young \(2006\)](#). Thus the changes in the ionization fractions since [Mazzotta et al. \(1998\)](#) shown in Figure 1 do not have a significant impact on the Mg/Ne ratio. The difference between the network and cell center values is only at the  $1.3 \sigma$  level, and if we use the average quiet Sun intensities we find a ratio of  $0.519 \pm 0.041$ . Applying a 20% uncertainty on the atomic data gives a final Mg/Ne ratio of  $0.519 \pm 0.112$ .

The Mg/Ne FIP bias in the quiet Sun depends on the choice of photospheric abundances. For the Asp-Sco abundance compilation, we update the neon abundance as described in the previous section, which gives a photospheric Mg/Ne ratio of  $0.326 \pm 0.084$ . The quiet Sun FIP bias is then  $1.59 \pm 0.54$ , and for the Lod-Caf abundance set it is  $1.68 \pm 0.62$ . For simplicity we can state the FIP bias as  $1.6 \pm 0.6$ , independently of which abundance set is used. We thus find a small FIP bias in the

upper transition region of the quiet Sun, although the ratio values are only  $1 \sigma$  above the photospheric ratios.

## 9. COMPARISON WITH CORONAL NE/O RESULTS

In this section we discuss recent progress in measuring the coronal Ne/O ratio. We first highlight that transition region emission is generally considered to come from dynamic structures that *are not physically connected to the corona* ([Feldman 1983](#)). Coronal structures pass through transition region temperatures as they connect to the photosphere, but this emission is much weaker than the disconnected structures. Direct evidence for these disconnected structures was recently presented from high spatial resolution UV observations obtained by the IRIS satellite ([Hansteen et al. 2014](#)), which also showed that they are highly dynamic with time-scales of minutes. If the physical mechanism that causes the FIP effect is assumed to operate over a period of time, then it is more likely that the dynamic transition region structures will show a smaller FIP bias than the longer-lived coronal structures, as recently suggested by [Warren et al. \(2016\)](#).

There have been several papers that have derived neon abundances from solar and stellar coronal spectra. [Landi et al. \(2007\)](#) and [Landi & Testa \(2015\)](#) used UV spectra from the Solar Ultraviolet Measurements of Emitted Radiation (SUMER) experiment on board SOHO to derive absolute neon abundances in off-limb coronal regions. The former work used a Ne IX line formed at 4 MK and produced during the decay phase of a solar flare. By comparing with the strength of the free-free continuum, a value of  $A(\text{Ne}) = 8.11 \pm 0.12$  was derived and this was used in the [Lodders et al. \(2009\)](#) abundance compilation.

A different approach was adopted by [Landi & Testa \(2015\)](#) who used lines of Ne VIII and O VI to measure the Ne/O ratio, and also used lines of H I to yield absolute abundances for Ne and O. The Ne VIII and O VI lines were measured in the off-limb corona where they are formed at about 1.3 MK, significantly higher than their  $T_{\text{max}}$  values of 0.63 and 0.28 MK, respectively, which is enabled by the extended high temperature tails of lithium-like ions. Abundances were derived from many datasets over the period 1996 to 2008, and time variations in the Ne/O ratio were found. Although the ratio was relatively constant during 1996–2005 (solar cycle 23), it rose significantly as the Sun entered the minimum of solar cycle 24. Interestingly, [Landi & Testa \(2015\)](#) argue that the high value of  $R_{\text{Ne/O}} = 0.25 \pm 0.05$ —a value consistent with that derived here—found at the end of the sequence in 2008 is the best representation of the

**Table 3.** Summary of abundance results.

Quantity	Value	
$R_{\text{Mg/Ne}}$	$0.519 \pm 0.112$	
$R_{\text{Ne/O}}$	$0.244 \pm 0.050$	
FIP bias (Mg/Ne)	$1.68 \pm 0.62$	(Lod-Caf)
	$1.59 \pm 0.54$	(Asp-Sco)
$A(\text{Ne})$	$8.15 \pm 0.10$	(Lod-Caf)
	$8.08 \pm 0.09$	(Asp-Sco)

true solar photospheric value due to the very low solar activity at this time, which may have depressed the FIP bias mechanism.

Drake (2011) reassessed the datasets studied by McKenzie & Feldman (1992) and Schmelz et al. (2005), processing Ne IX and O VIII X-ray line intensities to derive Ne/O ratios. Consistent with the earlier authors, he found evidence that the Ne/O ratio varies from dataset to dataset with an average close to the values from the Grevesse & Sauval (1998) and Asplund et al. (2009) datasets (and so lower than the value found here). A new result was the finding of a correlation with active region temperature. This was interpreted as supporting a result from stellar X-ray studies that the Ne/O ratio increases with stellar activity (Robrade et al. 2008). We note however, that this contradicts the result of Landi & Testa (2015) who suggested the Ne/O ratio is higher at times of low solar activity.

The conclusion that the coronal Ne/O varies from region to region and is possibly related to activity suggests that it is not a reliable measure of the photospheric ratio. The use of transition region data from quiet Sun in the present analysis is suggested here to be preferable, especially taking into account the low FIP bias found from Mg/Ne from the same datasets.

## 10. SUMMARY

The results from this work are summarized in Table 3. The Ne/O and Mg/Ne relative abundance ratios in the upper transition region of the quiet Sun have been re-evaluated by applying updated atomic data to previously published measurements. The key result is that the Ne/O ratio is 40% higher than found previously, a change driven by updates to the equilibrium ionization fractions of the neon and oxygen ions.

If we assume the quiet Sun Ne/O ratio represents the photospheric ratio, then the photospheric abundance of oxygen from Asplund et al. (2009) implies a neon abundance of  $A(\text{Ne}) = 8.08 \pm 0.09$ . If we use the higher oxygen abundance derived by Caffau et al. (2011), then we have  $A(\text{Ne}) = 8.15 \pm 0.10$ .

The Mg/Ne quiet Sun ratios are very similar to those derived by Young (2006), despite the updates in the ionization fractions. If we use the updated photospheric neon abundances found here, then a larger Mg/Ne FIP bias of  $1.6 \pm 0.6$  is found compared to the earlier work. This remains significantly smaller than the canonical FIP bias values of 4 and 3 used in the reviews of Feldman et al. (1992) and Schmelz et al. (2012), respectively. The abundance results are thus consistent with the notion that the observed transition region is predominantly disconnected from the corona.

The author acknowledges funding from NASA grants NNX15AF48G and NNX15AF25G. SOHO is a project of international cooperation between ESA and NASA. CHIANTI is a collaborative project involving George Mason University, the University of Michigan (USA) and the University of Cambridge (UK). The referee is thanked for valuable comments.

*Facilities:* SOHO(CDS)

*Software:* Solarsoft, CHIANTI

## REFERENCES

- Antia, H. M., & Basu, S. 2005, ApJL, 620, L129
- Arnaud, M., & Rothenflug, R. 1985, A&AS, 60, 425
- Asplund, M., Grevesse, N., Sauval, A. J., & Scott, P. 2009, ARA&A, 47, 481
- Bahcall, J. N., Basu, S., & Serenelli, A. M. 2005, ApJ, 631, 1281
- Bryans, P., Landi, E., & Savin, D. W. 2009, ApJ, 691, 1540
- Caffau, E., Ludwig, H.-G., Steffen, M., Freytag, B., & Bonifacio, P. 2011, SoPh, 268, 255
- Del Zanna, G., Andretta, V., Chamberlin, P. C., Woods, T. N., & Thompson, W. T. 2010, A&A, 518, A49
- Del Zanna, G., Dere, K. P., Young, P. R., Landi, E., & Mason, H. E. 2015, A&A, 582, A56
- Dere, K. P., Landi, E., Young, P. R., et al. 2009, A&A, 498, 915
- Doschek, G. A., & Laming, J. M. 2000, ApJL, 539, L71
- Drake, J. J. 2011, ApJ, 743, 22
- Drake, J. J., & Testa, P. 2005, Nature, 436, 525

- Dwivedi, B. N., Curdt, W., & Wilhelm, K. 1999, *ApJ*, 517, 516
- Feldman, U. 1983, *ApJ*, 275, 367
- Feldman, U., & Laming, J. M. 2000, *PhysS*, 61, 222
- Feldman, U., Mandelbaum, P., Seely, J. F., Doschek, G. A., & Gursky, H. 1992, *ApJS*, 81, 387
- Feldman, U., & Widing, K. G. 1993, *ApJ*, 414, 381
- Grevesse, N., & Sauval, A. J. 1998, *SSRv*, 85, 161
- Grevesse, N., Scott, P., Asplund, M., & Sauval, A. J. 2015, *A&A*, 573, A27
- Hansteen, V., De Pontieu, B., Carlsson, M., et al. 2014, *Science*, 346, 1255757
- Holweger, H. 1979, in *Liege International Astrophysical Colloquia*, Vol. 22, *Liege International Astrophysical Colloquia*, ed. A. Boury, N. Grevesse, & L. Remy-Battiau, 117–138
- Holweger, H. 2001, in *American Institute of Physics Conference Series*, Vol. 598, *Joint SOHO/ACE workshop “Solar and Galactic Composition”*, ed. R. F. Wimmer-Schweingruber, 23–30
- Landi, E., Del Zanna, G., Young, P. R., Dere, K. P., & Mason, H. E. 2012, *ApJ*, 744, 99
- Landi, E., Feldman, U., & Doschek, G. A. 2007, *ApJ*, 659, 743
- Landi, E., & Testa, P. 2015, *ApJ*, 800, 110
- Landi, E., Young, P. R., Dere, K. P., Del Zanna, G., & Mason, H. E. 2013, *ApJ*, 763, 86
- Lodders, K., Palme, H., & Gail, H.-P. 2009, *Landolt Börnstein*, 44
- Markwardt, C. B. 2009, in *Astronomical Society of the Pacific Conference Series*, Vol. 411, *Astronomical Data Analysis Software and Systems XVIII*, ed. D. A. Bohlender, D. Durand, & P. Dowler, 251
- Mazzotta, P., Mazzitelli, G., Colafrancesco, S., & Vittorio, N. 1998, *A&AS*, 133, 403
- McKenzie, D. L., & Feldman, U. 1992, *ApJ*, 389, 764
- Morel, T., & Butler, K. 2008, *A&A*, 487, 307
- Nikolić, D., Gorczyca, T. W., Korista, K. T., Ferland, G. J., & Badnell, N. R. 2013, *ApJ*, 768, 82
- Robrade, J., Schmitt, J. H. M. M., & Favata, F. 2008, *A&A*, 486, 995
- Schmelz, J. T., Nasraoui, K., Roames, J. K., Lippner, L. A., & Garst, J. W. 2005, *ApJL*, 634, L197
- Schmelz, J. T., Reames, D. V., von Steiger, R., & Basu, S. 2012, *ApJ*, 755, 33
- Scott, P., Asplund, M., Grevesse, N., Bergemann, M., & Sauval, A. J. 2015a, *A&A*, 573, A26
- Scott, P., Grevesse, N., Asplund, M., et al. 2015b, *A&A*, 573, A25
- Villante, F. L., Serenelli, A. M., Delahaye, F., & Pinsonneault, M. H. 2014, *ApJ*, 787, 13
- Warren, H. P., Brooks, D. H., Doschek, G. A., & Feldman, U. 2016, *ApJ*, 824, 56
- Young, P. R. 2005a, *A&A*, 439, 361
- . 2005b, *A&A*, 444, L45
- Young, P. R. 2006, in *ESA Special Publication*, Vol. 617, *SOHO-17. 10 Years of SOHO and Beyond*, 47.1
- Young, P. R., Dere, K. P., Landi, E., Del Zanna, G., & Mason, H. E. 2016, *Journal of Physics B Atomic Molecular Physics*, 49, 074009



## APPENDIX

## A. EFFECTS OF DR SUPPRESSION ON THE CHIANTI ION BALANCE FILE

Figure 1 showed the differences between the equilibrium ion fractions adopted in the present work and the ion fractions from [Mazzotta et al. \(1998\)](#) that were used by [Young \(2005a,b\)](#). In this appendix we highlight the effect caused by DR suppression on the current CHIANTI 8 zero-density equilibrium ion fractions, and in particular how it affects certain ions.

Figure 3 is an analogous plot to Figure 1, but comparing the ion fractions at  $P = 10^{14.5} \text{ K cm}^{-3}$  with the zero-density CHIANTI 8 file from which it is derived. Since the ionization rates are unaffected, the suppression of the DR rates results in the ion fraction curves moving to lower temperatures. This is most strongly seen for the oxygen ions, whereas the magnesium ions are relatively unaffected. The peaks of the ion fraction curves show changes of at most a few percent.

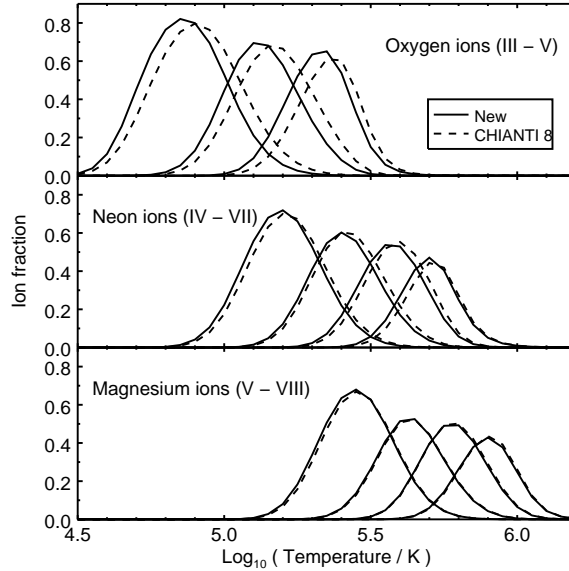


**Figure 3.** Ion fraction plots for the oxygen, neon and magnesium ions studied in the present work. The solid lines show the curves derived for a pressure of  $10^{14.5} \text{ K cm}^{-3}$ ; the dashed lines show the curves from distributed with CHIANTI 8.

Table 4 gives a list of the ions used in the present work, with their temperatures of maximum ionization ( $T_{\text{max}}$ ), and the factors,  $S$ , by which DR is suppressed at the ions'  $T_{\text{max}}$  values. The formulae of [Nikolić et al. \(2013\)](#) only correct an ion's DR rate above a certain density that is referred to as the activation density, and these values are also given in Table 4. We note that the activation density is lowest for the beryllium and boron-like ions (e.g., O V, O IV), and it increases with atomic number ( $Z$ ) along the sequence. A striking feature is that for all ions DR becomes suppressed at densities lower than typical solar atmosphere values ( $10^9 \text{ cm}^{-3}$ ), and so suppression is important to consider for studies of all solar features, particularly for  $Z \leq 10$ .

**Table 4.** DR suppression data for O, Ne and Mg ions.

Ion	$\text{Log}(T_{\text{max}}/\text{K})$	$\text{Log}(N_e/\text{cm}^{-3})$	$S(T_{\text{max}})$
O III	4.85	3.95	0.57
O IV	5.10	3.82	0.56
O V	5.35	3.22	0.53
Ne IV	5.20	5.42	0.79
Ne V	5.40	6.37	0.86
Ne VI	5.55	5.76	0.80
Ne VII	5.70	5.17	0.74
Mg V	5.45	6.66	0.89
Mg VI	5.65	7.45	0.95
Mg VII	5.80	8.09	0.98
Mg VIII	5.90	7.41	0.95